Grid Resolution for the Simulation of Sloshing using CFD

Bernhard Godderidge*, Mingyi Tan*, Chris Earl & Stephen Turnock***

*Fluid-Structures Interaction Research Group, School of Engineering Sciences, University of Southampton, Highfield, Southampton SO17 1BJ, UK
**BMT SeaTech, Grove House, 7 Ocean Way, Southampton SO14 3TJ, UK
Corresponding author's email: bg401@soton.ac.uk

Introduction

Sloshing occurs when a tank is partially filled with a liquid and subjected to an external excitation force [1]. Ships with large ballast tanks and liquid bulk cargo carriers, such as very large crude carriers (VLCCs), are at risk of exposure to sloshing loads during their operational life [2]. The inclusion of structural members within the tanks dampens the sloshing liquid sufficiently in all but the most severe cases. However, this approach is not used for Liquefied Natural Gas (LNG) carriers and the accurate calculation of the sloshing loads is an essential element of the LNG tank design process [3, 4].

The increase in global demand for LNG has resulted in a new generation of LNG tankers with a capacity in excess of 250,000 m^3, compared to 140,000 m^3 today. A prerequisite for the safe operation of these LNG tankers is an accurate calculation of the sloshing loads experienced by the containment system [5, 6].

The work of Abramson [7] summarizes the methods available in modern sloshing analysis, and Ibrahim [8] gives an up-to-date survey of analytical and computational sloshing modeling techniques. A more general modeling technique is the solution of the Navier-Stokes equations using Computational Fluid Dynamics (CFD). Some recent examples of CFD sloshing simulation include Hadzic *et al.* [9], Aliabadi *et al.* [10], Standing *et al.* [11], Kim *et al.* [12], Rhee [13] and El Moctar [14].

Sloshing flows are treated as a transient problem in CFD. While the number of sloshing oscillations can vary, a large number of time steps, usually $O(10^2)$ to $O(10^3)$ per oscillation are required. Design optimization or the use of a numerical wave tank to gather statistical sloshing pressure data [15] requires long simulation times or multiple runs. Parameters such as time step size, grid spacing and model choice directly influence the complexity and computational cost of a CFD model.

A sway-induced resonant sloshing flow in a 1.2 m x 0.6 m rectangular container is investigated using a commercial Navier-Stokes CFD code. The selected computational model was validated using experimental pressure data from Hinatsu [16] by Godderidge *et al.* [17, 18]. The effect of grid spacing when capturing impact pressure caused by an enclosed air bubble is investigated. It is found that local flow features are best suited to indicate that the flow is sufficiently well resolved. These findings are further investigated using larger, geometrically similar sloshing tanks. The initial grid geometry is used to simulate the scaled sloshing flow at two and four times the initial grid size. Then, the grid is refined to give the same mesh spacing as in the first problem.

Sloshing Problem

Sloshing in rectangular container, induced by pure sway motion, is investigated in the present study. Figure 1 shows the tank dimensions, locations of pressure monitor points and axis system orientation. The CFD model was validated using the experimental steady state sloshing pressures given by Hinatsu [16]. The tank displacement is given by

$$x = A\sin\left(\frac{2\pi}{T}\,t\right), \tag{1}$$

where A is the displacement amplitude, T the sloshing period and t the elapsed time. In the current case, the tank motion is in the x-direction only, as indicated in Figure 1. The first part of the investigation is focused on a resonant sloshing flow at 20% filling level, where $A = 0.06$ m and $T = 1.74$ sec. Subsequently, a near-resonant sloshing flow with $A = 0.015$ m and $T = 1.404$ sec is considered.

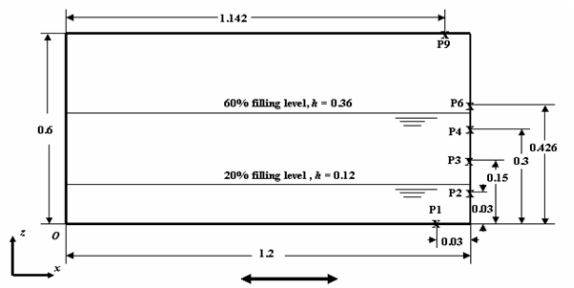

Figure 1: The sloshing problem used for CFD validation (all dimensions in m)

The fluid interaction models for the numerical simulation of sloshing can be implemented using the volume fraction of each fluid to determine the fluid mixture properties. This is a *homogeneous* multiphase model. It is analogous to the volume of fluid (VOF) method developed by Hirt and Nichols [19], but it includes a simplification as the free surface pressure boundary condition is neglected. A more general but computationally more expensive approach is an *inhomogeneous* multiphase model, where the solution of separate velocity fields for each fluid is matched at the fluid interfaces using mass and momentum transfer models [20]. An inhomogeneous viscous compressible multiphase flow with two phases α and β is governed by the conservation of mass for the compressible phase α

$$\frac{\partial}{\partial t}(r\rho) + \frac{\partial}{\partial x_i}(r\rho u_i) = m + \Gamma^{\alpha\beta}, \tag{2}$$

where $\Gamma^{\alpha\beta}$ is mass transfer between the phases and m mass sources, ρ density, r volume fraction and u_i velocity of phase α. The conservation of momentum for phase α is given as

$$\frac{\partial}{\partial t}(r\rho u_i) + \frac{\partial}{\partial x_j}(r\rho u_i u_j) = -r\frac{\partial p}{\partial x_i} + \\ + \frac{\partial}{\partial x_j}\left[r\mu\left(\frac{\partial u_i}{\partial x_j} + \frac{\partial u_j}{\partial x_i}\right)\right] + M^{\Gamma} + M^{\alpha} + b_i, \tag{3}$$

where b_i are body forces, M^{α} forces on the interface caused by the presence of phase β, μ the dynamic viscosity and the term $M^{\Gamma}\left(=\Gamma^{\alpha\beta}u_i^{\beta} - \Gamma^{\beta\alpha}u_i\right)$ interphase momentum transfer caused by mass transfer. If the fluid is compressible, Equations (2) and (3) are closed using an energy equation, or an equation of state if the compressible fluid can be treated as an ideal gas [21]. A discussion of the fluid interface forces is given by Godderidge *et al.* [22].

As a full set of conservation equations has to be solved for each phase, the computational effort required for the inhomogeneous model has been found to be 2.3 times greater[1] than for the homogeneous model [22]. However, Brennen [23] finds that if two conditions derived from particle size parameter, mass parameter and particle Reynolds number are violated, the inhomogeneous multiphase model (Equations 2 and 3) should be used. It is observed that for the current problem, the particle Reynolds number condition is not satisfied. This suggests that the use of an inhomogeneous multiphase model is required for the analysis of the current problem.

The computational models used in the sloshing studies are summarised in Table 1. The selection is based on the sensitivity study by Godderidge *et al.* [17]. It was found that the pressure histories of the current fluid model combination differed by less than 0.1% from the fully compressible model but required 20% less computational time. Kim *et al.* [12] showed that the sloshing pressure is not influenced by the inclusion of a turbulence model, but the use of a standard $k-\varepsilon$ turbulence model with a scalable wall function aided convergence when using a viscous flow model [17]. The high resolution scheme for spatial discretization varies between a first and second order upwind scheme depending on the gradient [21]. The grids used for the various studies are detailed in the sections describing the respective results.

[1]The simulations were run on a 64 bit, 2.2 GHz processor with 2 GB of RAM at the University of Southampton Iridis 2 computational facility

Table 1: Computational models used for sloshing simulations

Parameter	Setting
Water	Incompressible fluid
Air	Ideal gas
Multiphase model	inhomogeneous
Sloshing motion	Body force
Turbulence model	Standard $k-\varepsilon$ with scalable wall function
Spatial discretization	High resolution
Time discretization	Second order backward Euler
Timestep control	Root-mean-square (RMS) Courant number=0.1
Convergence control	RMS residual $< 10^{-5}$

The investigation of sloshing in geometrically similar containers required the calculation of an appropriate sloshing excitation. The nature of the excitation, given in Equation (1), is maintained but the amplitude and frequency are adjusted. The sloshing period is 95% of the resonant period which depends on the tank size. The resonant freqnecy for each case is calculated from potential theory as

$$\omega_n^2 = \frac{\pi g}{a}\tanh\left(\pi\frac{h}{a}\right), \tag{4}$$

where a is the tank length, g gravity and h the filling level. The amplitude of the sloshing excitation is adjusted using the sloshing velocity, which may be obtained by differentiating Equation (1). Taking the excitation velocity as a characteristic velocity, the following non-dimensional scaling parameter based on the Froude number [7] can be used

$$\frac{\dot{x_l}}{\dot{x_L}} = \frac{\sqrt{gD_l}}{\sqrt{gD_L}}, \tag{5}$$

where D_l and D_L are characteristic length scales.

Impact bubble

The fluid motion caused by sloshing results in static and dynamic pressure loads. The dynamic pressures are usually confined to small regions, but cause large loads on the structure. Sloshing pressure loads can be categorised as pure fluid impact, impact air bubble formation and the impact of an air-water mixture formed during a previous fluid impact. Pure fluid impact has been studied experimentally by Peregrine [24] and impact pressures in excess of 100 times the static fluid pressures were observed. The resonant sloshing flow results in a jet impacting the tank wall and subsequent air bubble entrainment. This tends to result in a longer, oscillating pressure history when compared to a pure fluid impact.

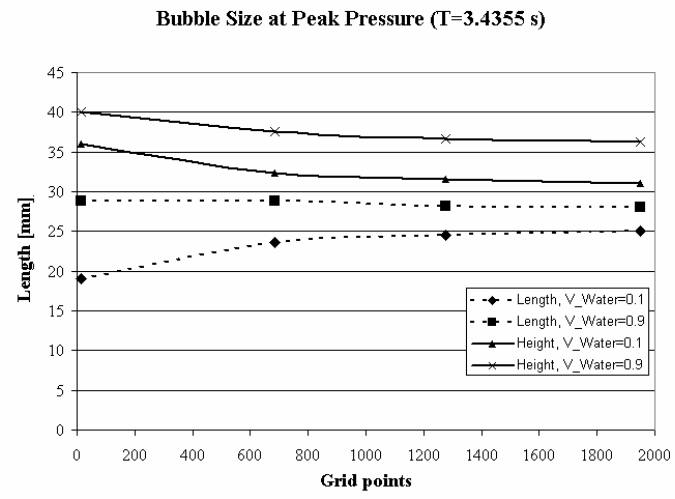

2(a): Bubble size dependence on grid

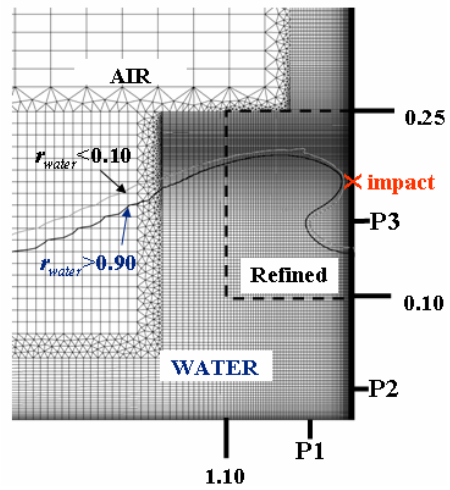

2(b): Air bubble formation

Figure 2: Air entrainment bubble formed during sloshing impact

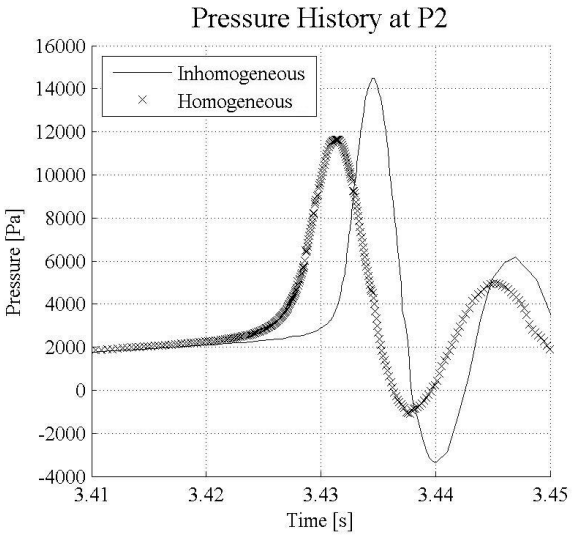

3(a): P2

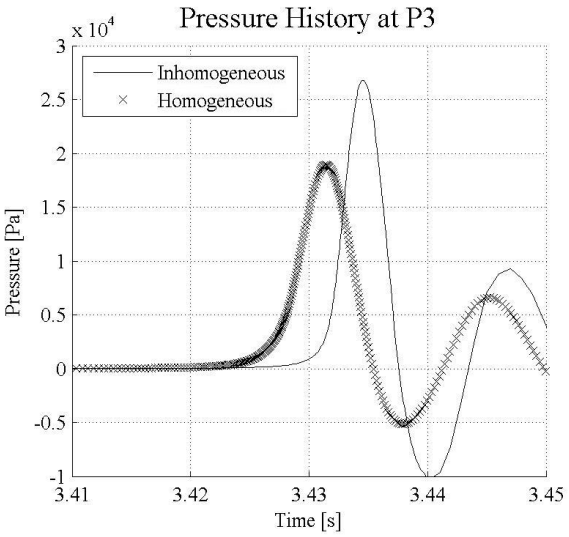

3(b): P3

Figure 3: Pressure history at P2 (left) and P3 (right)

The sloshing flow is simulated on a hybrid grid with a refined region indicated in Figure 2. Table 2 gives the grid particulars in the refined region. Figure 2(a) shows the grid dependence of the air bubble dimensions and the formation of the air bubble is illustrated in Figure 2(b).

Table 2: Grid refinement for sloshing impact

Grid	Hex.	horizontal (first node) (mm)	vertical (mm)
Grid a	408	0.30	12
Grid b	2552	0.10	3.5
Grid c	4602	0.05	2.0
Grid d	16284	0.02	0.5

Figure 3 shows the pressure history during fluid impact at P2 and P3 for the 20% filling level. In both cases, the homogeneous multiphase model gives, for the identical fluid model and initialisation, a significantly lower pressure than the inhomogeneous model. Figure 4 shows that the direction of the water prior to impact depends on the selected multiphase model. The inhomogeneous flow predicted water velocity is inclined 14.0° from the horizontal, while the homogeneous model estimated the velocity vector inclination at 40.3°.

The grid dependence of the calculated pressures is shown in Figure 5. The characteristic length scales are the length and depth for P1 and P2 are taken where the water surface is above its initial position The length and height of the bubble are the characteristic scales for P3 . Figure 5(a) shows the plot for the grid spacing perpendicular to the bottom wall for P1 and P2 and the side wall for P3. The grid spacing parallel to the wall is shown in Figure 5(b).

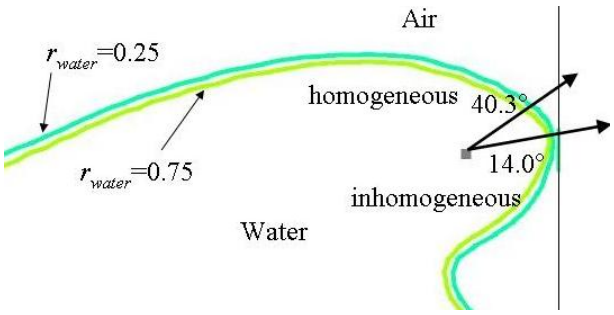

Figure 4: Water flow 0.05 cm before impact

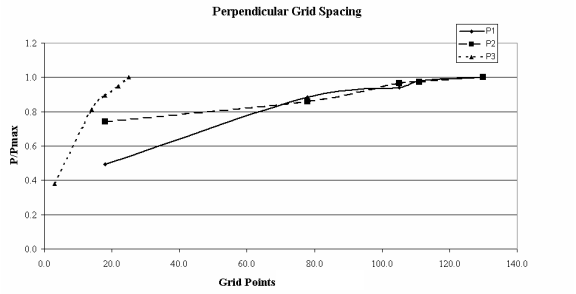

5(a): Perpendicular grid spacing

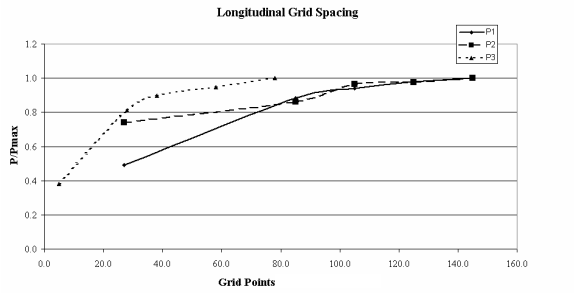

5(b): Longitudinal grid spacing

Figure 5: Pressure dependence on local perpendicular (top) and longitudinal (bottom) flow feature resolution

Tank Size Variation

Equation (1), which describes the sloshing excitation, can be rewritten as

$$x = \alpha A \sin\left(\frac{2\pi}{T}\, t\right), \tag{6}$$

where α is a constant. Using Equation (4) and (5), the sloshing excitation can be adjusted for kinematic similitude corresponding to the tank size. The computed values are given in Table 3.

The grid used for Case 1 which consists of 9360 elements is shown in Figure 6. Grid size and time discretisation parameters were determined from Ref [25]. This grid is then resized using the appropriate size factors for cases 2 and 3. The number of grid cells remains constant but the size of each element increases accordingly. A second set of grids (grid 2 and 3) is constructed for cases 2 and 3 respectively. They contain 38,319 and 153,273 elements respectively and they have the same cell size as the grid used for

Table 3: Systematic tank size variations

Parameter	Case 1	Case 2	Case 3
Sloshing Tank			
Size factor	1	2	4
Length	1.2 m	2.4 m	4.8 m
Height	0.6 m	1.2 m	2.4 m
Filling Level	60%	60%	60%
Excitation			
α	1	1.961	3.922
A	0.015 m	0.015 m	0.015 m
T_{10}	1.474 sec	2.044	2.890

case 1. The computational models used in the simulations are given in Table 1.

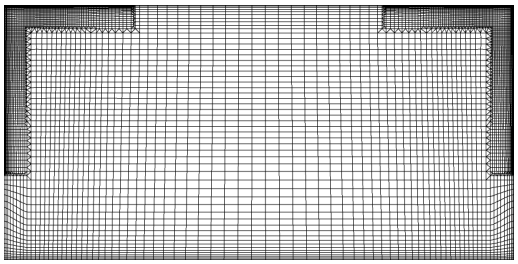

Figure 6: Typical hybrid grid used in CFD investigations. The grid contains 8652 hexahedral and 708 wedge elements

Figures 7(a) and 7(b) shows the pressure histories at monitor points P4 and P9 respectively for case 3 predicted using grids 1 and 3. At P4, which is dominated by the static pressure component, the pressure histories show reasonable agreement. At P9, the pressure spike captured on grid 3 is not observed using grid 1. Mean fluid speed is less susceptible to grid effects. Figures 7(c) and 7(d) show the mean fluid velocity, which is computed as

$$\text{Mean fluid speed} = \frac{\sum\limits_{mass} m_i |v_i|}{\sum\limits_{mass} m_i}. \tag{7}$$

Figure 7(c) shows acceptable agreement between the mean fluid speed history observed using grids 1 and 3. Finally, mean fluid speed appears to be a quantity well suited for scaling with Equation (5) as shown in Figure 7(d). While the scaled and observed speed histories are out of phase when using grid 1, the predicted magnitudes show good agreement with those observed when scaling from grid 2.

Concluding Remarks

The faithful discretisation of a sloshing problem in CFD depends on the resolution of local flow features. The most severe pressures were confined to small regions in the problem and occurred as a result of an impact jet and consequent air bubble entrapment. While the air bubble size was estimated accurately using a coarse grid, the grid independence of pressure requires a considerably finer grid. Thus, grid guidelines explicitly specifying grid spacing (e.g. Ref [26]) may not be adequate for sufficiently accurate computations. A better approach is to use a coarse

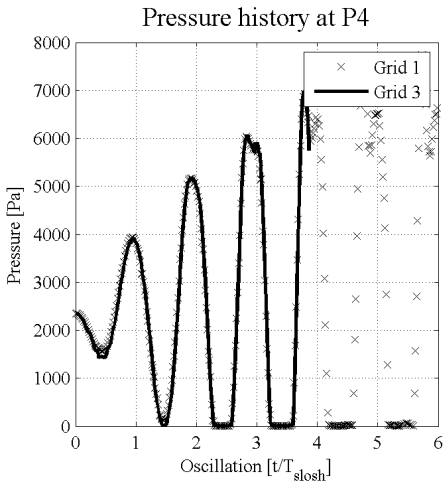

7(a): Pressure at P4

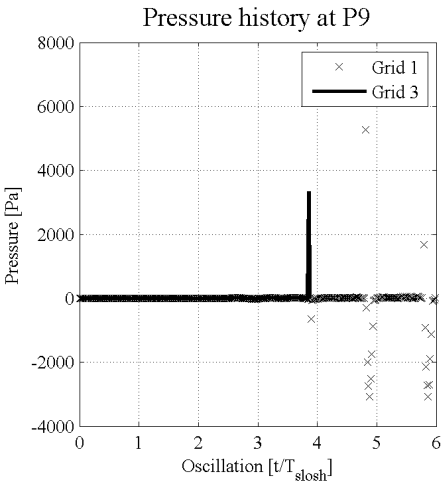

7(b): Pressure at P9

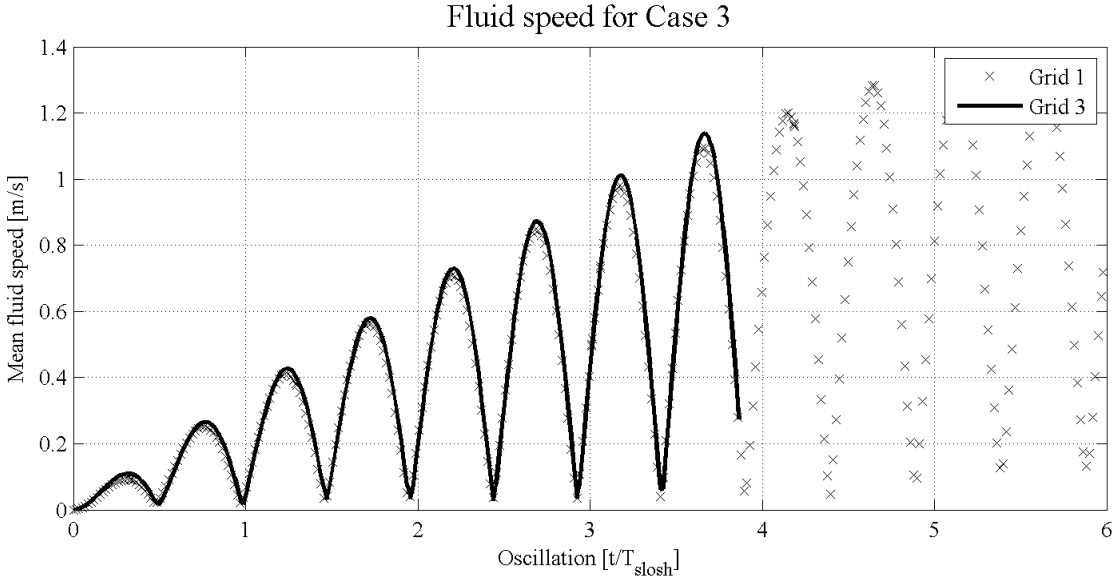

7(c): Grid dependence of fluid momentum

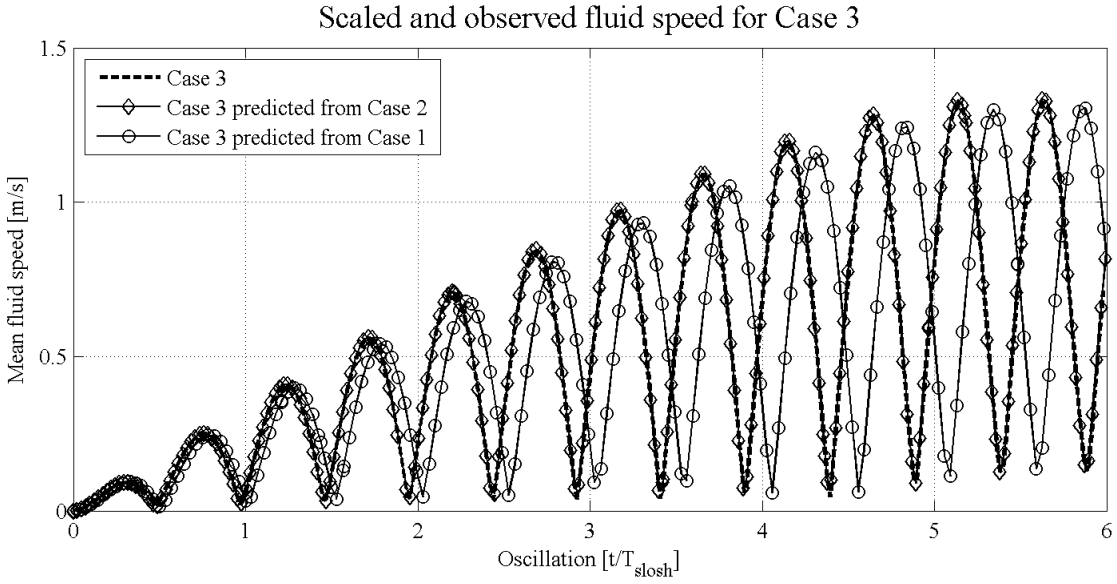

7(d): Predicted and observed fluid momentum

Figure 7: Grid influence on and scaling of fluid momentum

grid to observe critical flow features and repeat the simulation on a grid that adequately resolves local flow features by including information from e.g. Ref [27].

When increasing the tank size, local impact pressures are not captured unless the grid is refined according to the flow field. Moreover, the scaling of sloshing pressures remains a task of some difficulty. The mean fluid velocity defined in Equation (7) appears to be a quantity better suited to scaling. The magnitude of the mean fluid velocity of case 3 is estimated with good accuracy based on grids 1 or 2. However, a lag develops between the solution estimated from grid 1 and the mean fluid momentum obtained from grid 3.

The scaling of mean fluid velocity requires further study for additional validation. The simulations for the systematic variations of tank size should be extended to at least 10 oscillations. A further tank size of 9.6 m by 4.8 m should be included to confirm the scaling properties of mean fluid momentum. Ultimately, the mean fluid velocity may provide an alternative design criterion more suitable for scaling when assessing the safety of LNG tanks.

References

[1] Harald Olsen. What is sloshing? In *Seminar on Liquid Sloshing*. Det Norske Veritas, 1976.

[2] E Rizzuto and R Tedeschi. Surveys of actual sloshing loads onboard of ships at sea. In *NAV 97: International Conference on Ship and Marine Research*, 1997.

[3] Robert L Bass, E B Bowles, and P A Cox. Liquid dynamic loads in LNG cargo tanks. *SNAME Transactions*, 88:103–126, 1980.

[4] T Knaggs. New strides in ship size and technology. *Gas Ships: Trends and Technology.*, 2:1–4, 2006.

[5] Sungkon Han, Joo-Ho Heo, and Sung-Geun Lee. Critical design issues of new type and large LNG carriers. In *Proceedings of the 15th International Offshore and Polar Engineering Conference*, 2005.

[6] James Card and Hoseong Lee. Leading technology for next generation of LNG carriers. In *Proceedings of the 15th International Offshore and Polar Engineering Conference*, 2005.

[7] H Norman Abramson. The dynamic behavior of liquids in moving containers, with applications to space vehicle technology. Technical Report SP-106, National Aeronautics and Space Administration, 1966.

[8] Raouf A Ibrahim. *Liquid Sloshing Dynamics*. Cambridge University Press, 2005.

[9] I Hadzic, Frank Mallon, and M Peric. Numerical simulation of sloshing. Technical report, Technische Universität Hamburg-Harburg, 2002.

[10] Shahrouz Aliabadi, Andrew Johnson, and Jalal Abedi. Comparison of finite element and pendulum models for simulation of sloshing. *Computers and Fluids*, 32:535–545, 2003.

[11] R G Standing, S Amaratunga, F Lopez-Calleja, S Orme, and R Eichaker. Marine hydrodynamics modelling using CFD. In *CFD 2003: Computational Fluid Dynamics Technology in Ship Hydrodynamics*, 2003.

[12] Yonghwan Kim, Jungmoo Lee, Young-Bum Lee, and Yong-Soo Kim. Sensitivity study on computational parameters for the prediction of slosh-induced impact pressures. In *Proceedings of the 15th International Offshore and Polar Engineering Conference*, 2005.

[13] Shin Hyung Rhee. Unstructured grid based Reynolds-Averaged Navier-Stokes method for liquid tank sloshing. *Transactions of the American Society of Mechanical Engineers*, 127:572–582, 2005.

[14] Ould El Moctar. Assessment for tankers. *Shipping World and Shipbuilder*, 204:28–31, 2006.

[15] Mateusz Graczyk, Torgeir Moan, and Olav Rognebakke. Probabilistic analysis of characteristic pressure for LNG tanks. *Journal of Offshore Mechanics and Arctic Engineering*, 128:133–144, 2006.

[16] Munehiko Hinatsu. Experiments of two-phase flows for the joint research. In *Proceedings of SRI-TUHH mini-Workshop on Numerical Simulation of Two-Phase Flows*. National Maritime Research Institute & Technische Universität Hamburg-Harburg, NMRI, 2001.

[17] Bernhard Godderidge, Mingyi Tan, and Stephen Turnock. A verification and validation study of the application of computational fluid dynamics to the modelling of lateral sloshing. Ship Science Report 140, University of Southampton, 2006.

[18] Bernhard Godderidge, Mingyi Tan, Stephen Turnock, and Chris Earl. Multiphase CFD modelling of a lateral sloshing tank. In *Numerical Towing Tank Symposium*, 2006.

[19] C W Hirt and B D Nichols. Volume of fluid (VOF) method for the dynamics of free boundaries. *Journal of Computational Physics*, 39:201–225, 1981.

[20] M Ishii and T Hibiki. *Thermo-Fluid Dynamics of Two-Phase Flow*. Springer Verlag, 2006.

[21] Ansys Inc. *CFX-10 User's Guide*, 2005.

[22] B Godderidge, S Turnock, M Tan, and C Earl. An investigation of multiphase CFD modelling of a lateral sloshing tank. *Computers and Fluids (submitted)*.

[23] C E Brennen. *Fundamentals of Multiphase Flow*. Cambridge University Press, New York, 2005.

[24] Wu-Ting Tsai and Dick K. P Yue. Computation of nonlinear free surface flows. *Annual Review of Fluid Mechanics*, 28:249–278, 1996.

[25] B Godderidge, M Tan, C Earl, and S Turnock. Boundary layer resolution for modeling of a sloshing liquid. In *International Society of Offshore and Polar Engineers*, 2007.

[26] American Bureau of Shipping. Guidance notes on strength assessment of membrane-type LNG containment systems under sloshing loads. Technical report, American Bureau of Shipping, 2006.

[27] Joe F Thompson, Bharat K Soni, and Nigel P Weatherill, editors. *Handbook of Grid Generation*. CRC Press, 1999.